

Optical properties of materials for magnesium plasmonics described within DFT+U approach

© V.A. Durymanov, L.A. Avakyan, V.V. Srabionyan, D.S. Rubanik, L.A. Bugaev

Southern Federal University,
344006 Rostov-on-Don, Russia

e-mail: durymanov@sfedu.ru

Received April 01, 2023

Revised September 26, 2023

Accepted September 28, 2023

The most widely used and applied plasmonic materials, namely silver and gold, has limitations due to their high cost and restriction on the spectral position and shape of the plasmon resonance. This remains true for bimetallic silver-gold nanoparticles. Higher flexibility is required, in particular, for the design of broadband absorbers of light, and for this task the metals other than silver and gold are considered. In this paper we study the optical extinction spectra of alloy and composite nanoparticles containing magnesium and gold. The dielectric properties are calculated within the approximation of independent particles (IPA) based on the electronic structure obtained using density functional theory (DFT) with Hubbard correction (DFT+U). The obtained spectra of optical extinction of magnesium-gold alloy nanoparticles demonstrate that the most sensitive to the composition is the region of wavelengths below 500 nm. Simultaneously, the position of the plasmon resonance predicted by Vegard's law is higher than obtained from accurate DFT+U based calculations. We managed to describe the experimental optical extinction spectra of the glass sample containing gold and magnesium atoms using the calculated spectra. The results points on the formation of composite nanoparticles with core of Au₃Mg alloy and shell of Au in the considered sample.

Keywords: Density functional theory with Hubbard correction, optical extinction spectra, MgAu alloys, localized surface plasmon resonance.

DOI: 10.61011/EOS.2023.09.57351.4777-23

1. Introduction

Plasmonic materials are now used widely in various branches of activity [1], including structural surface-enhanced Raman scattering (SERS) studies [2,3], conversion of light energy into heat [4], medical imaging [5], catalysis [6], photovoltaics, and optoelectronics [7]. The unique optical properties [8–10] of materials based on gold and silver nanoparticles have made them the most widespread of all plasmonic ones. However, the high cost of these plasmonic materials based on monometallic gold and silver nanoparticles is their major disadvantage. Other plasmonic metals and alloys, such as copper [11], aluminum oxide, gallium, and magnesium [12–14], are regarded as possible alternatives. These metals are more commonly occurring and relatively inexpensive, but are also far less resistant to oxidation, which may induce degradation of the optical properties of materials based on them. The fundamental restriction on positioning and width of the localized surface plasmon resonance (LSPR) peak is another drawback common to all materials based on monometallic plasmonic nanoparticles. This restriction makes it more difficult to use them for the design of broadband absorbers aimed at converting light into heat, energy accumulation and transport, the construction of selective absorbers adjustable within a wide wavelength range, etc.

The fabrication of bimetallic nanoparticles with both core-shell [15,16] and alloy/solid solution [17,18] structures is one of the possible ways to overcome the mentioned constraints. The resultant LSPR in such bimetallic nanoparticles with components having widely different LSPR energies may be adjusted within a wide range (bounded by LSPRs of each component) by varying the component composition and the atomic architecture of particles (i.e., the nature of distribution of components over the particle volume). This approach to synthesis of bimetallic gold-silver nanoparticles with a core-shell structure has been implemented in [19]. It was demonstrated that the resultant LSPR band may be positioned anywhere within the range from ~ 450 to 600 nm, which is several times wider than the range of LSPR adjustment for monometallic nanoparticles performed by varying their size.

Recent reports on the potential application of relatively large (greater than 100 nm) magnesium nanoparticles in broadband light absorbers [14] and the positioning of the LSPR band of monometallic magnesium nanoparticles with a diameter of ~ 50 nm, which is located at wavelengths $\lambda \sim 350$ nm, suggest that more readily available magnesium is a viable substitute for expensive silver in gold-silver nanoparticles with a core-shell structure designed to be used in both broadband and selective light absorbers. However, one should bear in mind that probable structural instabilities with respect to component mixing [20] make it virtually impossible to obtain an ideal core-shell structure

in experiments. This factor should also be taken into account in the analysis of bimetallic nanoparticles. However, it should be noted here that recent data on gold–silver nanoparticles [21] reveal that nanomaterials of this kind with core–shell structures and alloys have different patterns of variation of plasmonic properties with component concentrations. This result suggests the possibility of determination of the structure of bimetallic nanoparticles based on their optical extinction spectra and underscores once again the significance of examination of plasmonic materials with a doped structure.

Although bimetallic nanoparticles based on gold and magnesium have application potential, a directed search for novel plasmonic materials of this type and estimation of their expected optical properties require data on the dielectric properties (complex refraction index) of alloys of gold and magnesium. These data are incomplete or, in certain cases, entirely absent.

The present study is focused on the determination of dielectric functions of a series of alloys with $\text{Au}_x\text{Mg}_{1-x}$ ($x = 0.25, 0.33, 0.5, 0.75$) compositions via ab initio calculations performed using density functional theory (DFT) with a Hubbard correction (DFT+U). The obtained dielectric functions are used to calculate the extinction spectra of MgAu nanoparticles in glass, which are then compared to the experimental spectral for synthesized samples. The methods and approaches to calculation of the electron structure and the dielectric properties of alloys and the extinction spectra for nanoparticles are discussed in Section 2. The obtained results are presented and analyzed in Section 3, and the key findings are summarized in Section 4.

2. Methods and approaches

The DFT+U approach has already been used [22] to predict the optical properties of plasmonic materials: certain binary alloys of gold, magnesium, silver, and aluminum. However, only one alloy ($x = 0.5$) with the smallest periodic cell from the $\text{Au}_x\text{Mg}_{1-x}$ series has been examined. Alloys with larger cells are analyzed in the present study, which is also distinct in that a more widespread, free, and open-source software package (Quantum Espresso, QE [23]) with an active community is used in it. QE is updated constantly and is on par in terms of features with commercial software. Specifically, QE does not only support self-consistent cycles of electron structure optimization within the LDA (local density approximation) +U approach, but also provides an opportunity to perform ab initio calculations of Hubbard parameter U [24], potentially allowing one to analyze advanced materials that have no experimental data available for them. The differences between QE and GPAW [25] related to the implementation of Kohn–Sham equations solving algorithms, the internal representation of electron densities, the pseudopotential form, and the method for calculation of the dielectric function or the system response to an external electric field

make it necessary to perform justification for the choice of Hubbard correction U .

Structural data on gold, magnesium, and their alloys were taken from the COD database [26]. Wave functions in the QE approach were expanded in a plane-wave basis. The basis size was defined by the highest kinetic energy of a plane wave, which was set to 545 eV as a result of convergence tests for the total energy and the Fermi energy. The states of core electrons were accounted by optimized norm-conserving Vanderbilt pseudopotentials [27]. To improve the convergence of the self-consistency procedure, the occupation numbers of states were characterized by a distribution similar to the Fermi–Dirac one with smearing parameter $\sigma = 0.01$ eV.

The stability of examined compounds (energetic advantage of formation of a material with an alloy structure over the emergence of elementary phases of its components) was estimated by analyzing per-atom formation energies E_f defined as

$$E_f = (E^{\text{alloy}} - N_A\mu_A - N_B\mu_B)/(N_A + N_B),$$

where E^{alloy} is the energy of a cell containing N_A and N_B atoms of types A and B, respectively. The formation energy of a stable compound should be negative. Chemical potentials μ_A were estimated as the total energy per-atom ($\mu_A = E_A^{\text{cryst}}/N$) of a crystal in the standard phase of atoms A (a face-centered cubic (FCC) crystal for Au and a close-packed hexagonal (HCP) crystal for Mg).

Self-consistent calculations of the electron structure of a primitive gold cell (cell parameter $a = 4.07$ Å) were carried out with a $15 \times 15 \times 15$ k -point grid. The electron structure of pure magnesium and AuMg alloys was determined using a k -point grid with a density equivalent to the point density in calculations for pure gold; in the case of HPC magnesium, the size of this grid is $23 \times 23 \times 12$.

Dielectric functions (ϵ) were calculated within the random phase approximation (RPA) that is implemented in the epsilon.x code, which is a part of the QE package [23]. The energies and wave functions of states needed for the calculation of dielectric functions were estimated in a non-self-consistent fashion based on the self-consistent density of occupied states. Denser k -point grids with approximately the same density corresponding to all materials were used for this purpose. Specifically, a $27 \times 27 \times 27$ grid was used for gold. The number of unoccupied states was chosen so as to leave no less than four unoccupied states per a single gold atom and no less than three unoccupied states per a magnesium atom. The dielectric function of pure magnesium was calculated within LDA without Hubbard correction U , since no d states are occupied in this case.

Complex refraction index $n_c = n + ik$ was calculated based on the dielectric function as

$$n = \sqrt{(|\epsilon| + \epsilon_1)/2}, \quad k = \sqrt{(|\epsilon| - \epsilon_1)/2}.$$

Optical extinction spectra for spherical nanoparticles and composite core–shell (core@shell) nanoparticles were

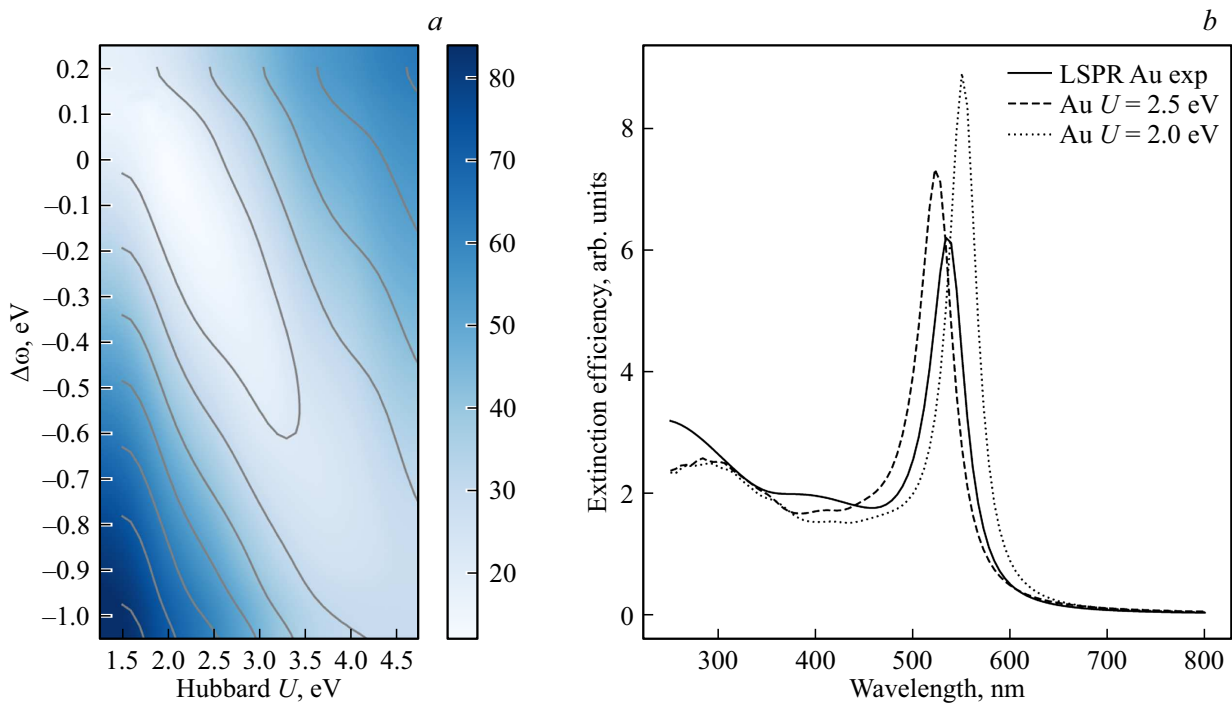


Figure 1. (a) Dependence of residual χ^2 on Hubbard parameter U and shift $\Delta\omega$. (b) Comparison of the optical extinction spectra of gold nanoparticles 30 nm in diameter in a glass matrix calculated with the use of different dielectric functions: the experimental function of Rioux et al. [31] (solid curve) and functions with parameters $U = 2.5$ and 2.0 eV (dashed and dotted curves, respectively).

modeled using the multi-sphere T-matrix method [28] with the MSTM-Studio Python interface [29]. The size of nanoparticles in models was set to 30 nm, which corresponds to diameters of the largest nanoparticles introduced into glass in an experiment on laser melting of a gold film [19]. The refraction index of the matrix was set to 1.5, which corresponds to optical glasses.

3. Discussion and results

3.1. Selection of parameter U for the Hubbard correction

Although the Hubbard correction parameter for pure gold has already been chosen in the previous study, the obtained values cannot be used directly in QE [30]. The calculation of parameter U from linear-response theory [24] requires considerable computational resources and may lead to suboptimal characterization of experimental spectra.

In the present study, parameter U was chosen by comparing the imaginary parts of experimental $\varepsilon_2^{\text{exp}}$ and theoretical $\varepsilon_2^{\text{theor}}$ dielectric functions. The similarity between them was characterized by residual χ^2 defined as

$$\chi^2 = \left(\varepsilon_2^{\text{exp}}(\omega) - \varepsilon_2^{\text{theor}}(\omega + \Delta\omega, U) \right)^2,$$

where $\Delta\omega$ is the additional shift of the dielectric function in the frequency ω scale. The residual value of $\Delta\omega = 0$ indicates on direct proximity of compared functions, while

the „shape“ similarity of dielectric functions is evaluated at nonzero shift $\Delta\omega$ to offset the shift between them associated with the imperfection of the exchange-correlation functional. The data from [30] for pure gold were used as the experimental ones. Figure 1, a presents the calculated dependence of this residual on Hubbard parameter U and additional shift $\Delta\omega$. It can be seen from Fig. 1, a that the residual is minimized at $U = 2.0 - 2.5$ eV. The extinction spectra of nanoparticles (spectra for a gold nanoparticle with a diameter of 30 nm in glass are shown as an example in Fig. 1, b) demonstrate that the dielectric functions calculated with $U = 2.5$ eV with no additional shift $\Delta\omega$ are preferable. The obtained U value was used in subsequent calculations for gold atoms in all the examined materials.

3.2. Simulation results for elementary metals

Before examining the alloys, let us make sure that the DFT+ U approach implemented in QE is applicable to the calculation of dielectric functions of elementary metals. Figures 2, a, b present the comparison of calculated complex refractive indices of pure gold and magnesium with the experimental data obtained by Rioux et al. [31] (for gold) and Hagemann et al. [32] (for magnesium). It is evident that a qualitative agreement the theoretical and experimental functions, which could not be achieved for gold within the common DFT approach, was reached. Note that the remaining discrepancies between the experimental

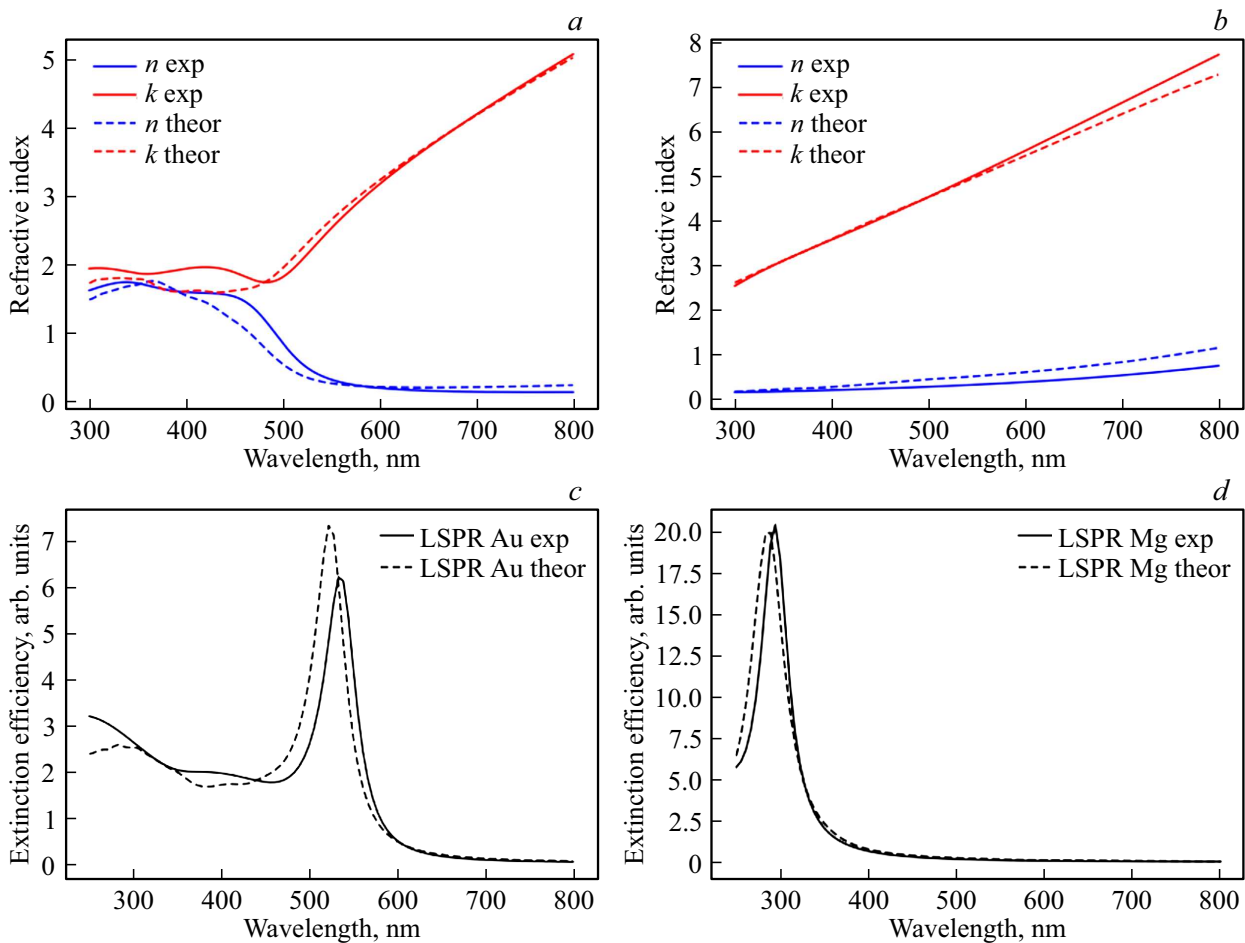


Figure 2. Comparison of the calculated complex refractive indices of (a) gold and (b) magnesium (dashed curves) with the experimental data (solid curves) obtained by (a) Rioux et al. [31] and (b) Hagemann et al. [32]. The results of calculation of optical extinction spectra of spherical (c) gold and (d) magnesium nanoparticles 30 nm in diameter in a dielectric matrix with $n = 1.5$ with the use of refraction indices from panels (a), (b) are presented at the bottom.

and theoretical functions do not translate into any marked differences between experimental and theoretical plasmon resonance spectra. This is illustrated by Figs. 2, c, d where the calculated extinction spectra for nanoparticles 30 nm in diameter are shown. It is evident that the error of determination of the LSPR maximum position is $\sim 2\%$ for both gold and magnesium, and the errors of estimation of the extinction maximum are $\sim 18\%$ and $\sim 2\%$ for gold and magnesium, respectively.

3.3. Simulation results for alloys

Data on the atomic structure of $\text{Au}_x\text{Mg}_{1-x}$ alloys with various gold concentrations $x = 0.25, 0.33, 0.5, 0.75$ were taken from the COD crystallographic database [26] without optimization of lattice parameters (to make them closer to the experimental data). A hypothetical AuMg structure with a NaCl-type lattice was taken as the initial one, and the cell parameter was optimized for it. The same Hubbard correction $U = 2.5$ eV was introduced for all gold atoms. The obtained alloy formation energies are listed in the table.

All of them are negative, indicating that the alloys are stable and the calculated data are correct. Since the formation energy for the AuMg alloy (with a CsCl structure) turned out to be the lowest, this alloy should be the most likely to form if gold and magnesium are present in the required proportion. Although the hypothetical alloy with a NaCl-type structure also has a negative formation energy, it is 0.029 eV/atom higher than the one for the alloy with a CsCl-type structure. Note that alloys with a high concentration of gold (above 50 at.%) should be the ones best suited for the design of broadband light absorbers [22].

Figures 3, a, c, e, g present the results of calculation of complex refractive indices of bulk $\text{Au}_x\text{Mg}_{1-x}$ alloys at $x = 0.25, 0.33, 0.5, 0.75$, while Figs. 3, b, d, f, h show the corresponding extinction spectra for gold nanoparticles with a diameter of 30 nm in glass that are formed from alloys with the calculated refraction indices. Comparing these data with Fig. 2, one finds that the refraction indices are much closer to those of magnesium than to the indices of gold. This is reflected in the plasmonic properties of nanoparticles. Specifically, the plasmon resonance of

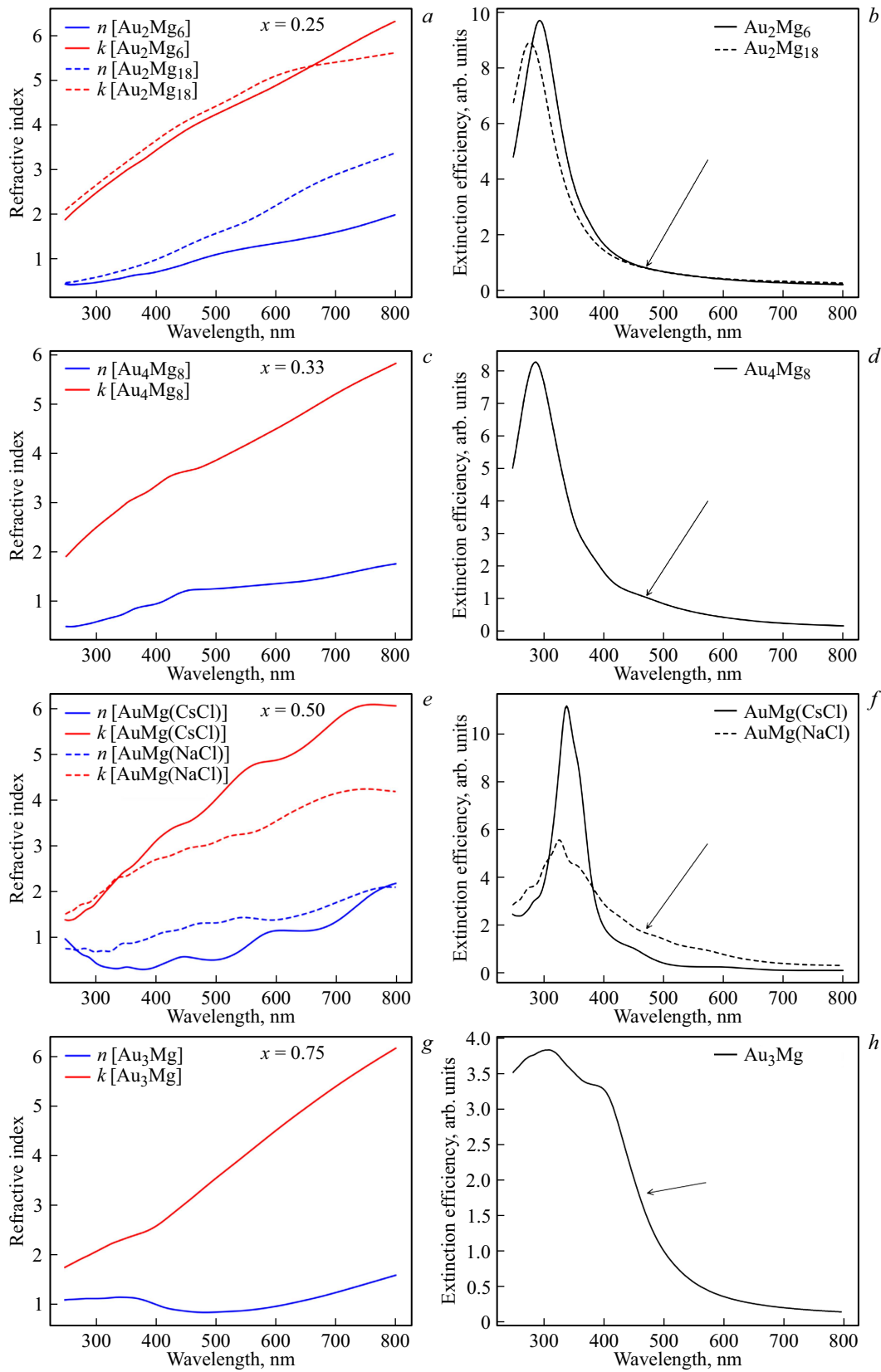
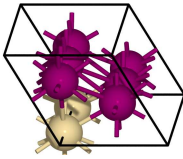
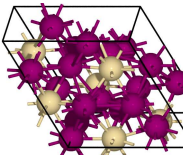
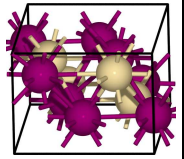
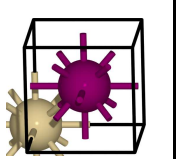
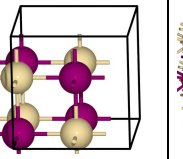
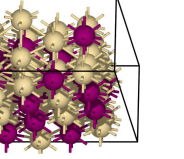


Figure 3. Comparison of the calculated complex refractive indices of $\text{Au}_x\text{Mg}_{1-x}$ alloys with various gold concentrations $x = 0.25, 0.33, 0.5, 0.75$ (a, c, e, g). Panels b, d, f, and h present the results of calculation of optical extinction spectra of nanoparticles 30 nm in diameter in a dielectric matrix with $n = 1.5$, which have the compositions of the corresponding $\text{Au}_x\text{Mg}_{1-x}$ alloys. Arrows point at the bumps attributed to the contribution of gold.

Formation energies for the examined alloys and illustrations of the corresponding structures

Illustration of the structure						
Alloy	Au ₂ Mg ₆	Au ₆ Mg ₁₈	Au ₄ Mg ₈	AuMg(CsCl type)	AuMg(NaCl type)	Au ₃ Mg
COD ID	1510237	1510235	1510233	9008804	–	1510506
Symmetry	<i>P63/mmc</i>	<i>P – 3c1</i>	<i>Pnma</i>	<i>Pm3m</i>	<i>Fm – 3m</i>	<i>Cmcm</i>
Au:Mg	1:3	1:3	1:2	1:1	1:1	3:1
E_f , eV/Atom	–0.009	–0.029	–0.035	–0.045	–0.016	–0.030

these nanoparticles is located in the UV region and its positioning depends only weakly on the gold concentration in a particle, indicating that the magnesium contribution is dominant. The LSPR intensities also depend weakly on the fraction of gold in all the examined alloys; the sole exception is AuMg with a NaCl-type structure, which exhibits an almost twofold reduction in intensity. As the gold concentration increases, a bump emerges and grows within the 400–500 nm wavelength interval. These bumps, which are denoted with arrows in Figs. 3, *b, d, f, h*, represent the contribution of gold. It is evident that the refraction index of the Au₃Mg alloy (Fig. 3, *g*) has more pronounced features associated with gold (300–400 nm). Just as in the NaCl-type AuMg alloy, the LSPR intensity for Au₃Mg nanoparticles undergoes an almost twofold reduction relative to the compositions containing fewer gold atoms. At the same time, considerable broadening of the LSPR band (from 300–400 nm for AuMg with a CsCl structure to ~ 200 – 450 nm) is observed. This broadening is the result of growth of the bump associated with the contribution of gold.

The obtained results verify the assumption made in [22] that the use of Au_{*x*}Mg_{1–*x*} nanoparticles of moderate sizes (≤ 60 nm) and a gold concentration below 50 at.% should not be a feasible route to absorption within a wide wavelength range, while Au_{*x*}Mg_{1–*x*} nanoparticles containing more than 50 at.% Au hold promise for the design of broadband light absorbers.

3.4. Applicability of the Vegard's law in determination of the LSPR position

The applicability of the Vegard's law in determination of the LSPR position for gold–silver nanoparticles has been considered in [21]. As was expected, the resonance position for nanoparticles formed from disordered AuAg alloys follows this linear law rather closely. Let us examine the case of ordered alloys of gold and magnesium. Figure 4 shows the variation of position of the plasmon resonance

peak in Au_{*x*}Mg_{1–*x*} alloys with gold concentration. It can be seen that the LSPR positions predicted for alloys are well below the curve representing a linear behavior consistent with the Vegard's law. This differs from the results obtained for nanoparticles formed from AuAg alloys and core–shell AuAg nanoparticles [21]. The LSPR band position remains almost unchanged (the deviation is < 5%) as the gold concentration increases up to 33%; therefore, one cannot adjust the resonance position in nanoparticles of this kind by varying their composition.

3.5. Characterization of the experimental extinction spectrum of the AuMg/glass sample

The calculated optical properties of AuMg alloys provide an insight into the structure of real materials. Let us consider an example extinction spectrum for a sample prepared by irradiating a thin film, which was positioned on glass and contained gold and magnesium, by a nanosecond laser (100 pulses, each with a mean fluence of 100 mJ/cm²). Since Au and Mg were present in the initial film, it is to be expected that nanoparticles produced under irradiation should also contain these metals [19].

Since magnesium may evaporate completely or oxidize and lose its plasmonic properties, an attempt at characterizing the extinction spectrum of the produced composite material with contributions of just the gold nanoparticles taken into account was made first. Figure 5, *a* presents the result of fitting the experimental extinction spectrum with model contributions of gold nanoparticles with their sizes distributed lognormally [33]. The distribution parameters and the constant background contribution were varied to obtain the best fit to the experimental curve. As one can see, the experimental spectrum deviates considerably from the theoretical curve plotted under the assumption that gold nanoparticles are the only ones present in the sample. This assumption also led to an unrealistic

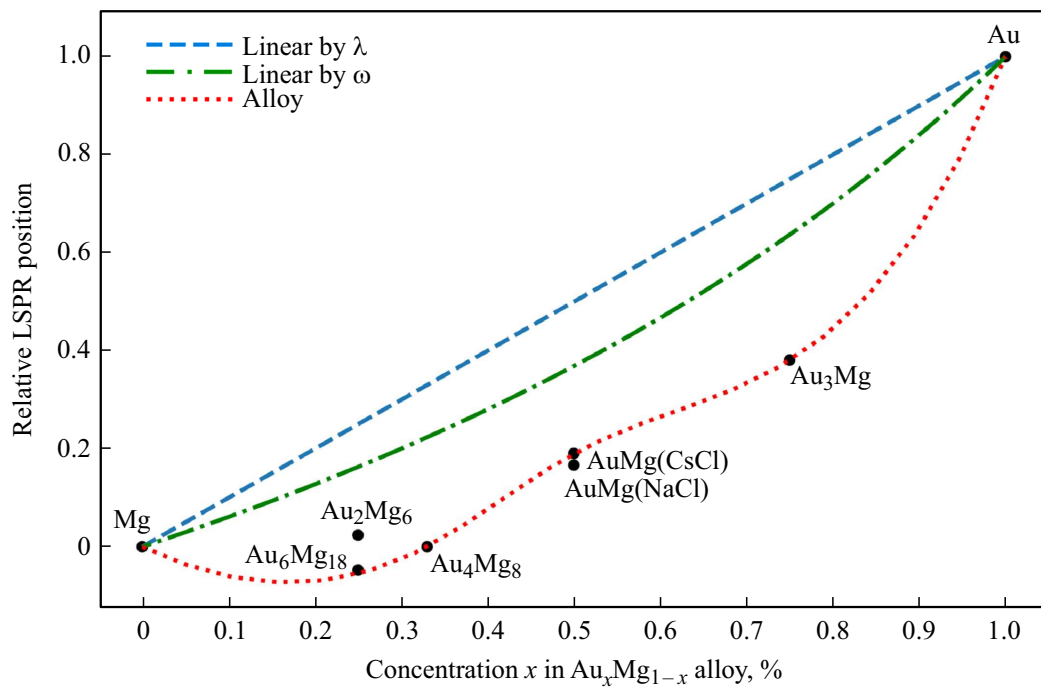


Figure 4. Dependences of the relative position of plasmon resonance on the concentration of gold in Au_xMg_{1-x} alloys for nanoparticles 50 nm in diameter in a dielectric matrix with $n = 1.5$ (dots). The Vegard’s law is illustrated by two curves: the dashed one corresponds to a linear concentration dependence of the LSPR position in the wavelength domain, while the dash-and-dot curve corresponds to a linear dependence in the frequency domain. The dotted interpolation curve goes through data points for alloys with the lowest formation energy.

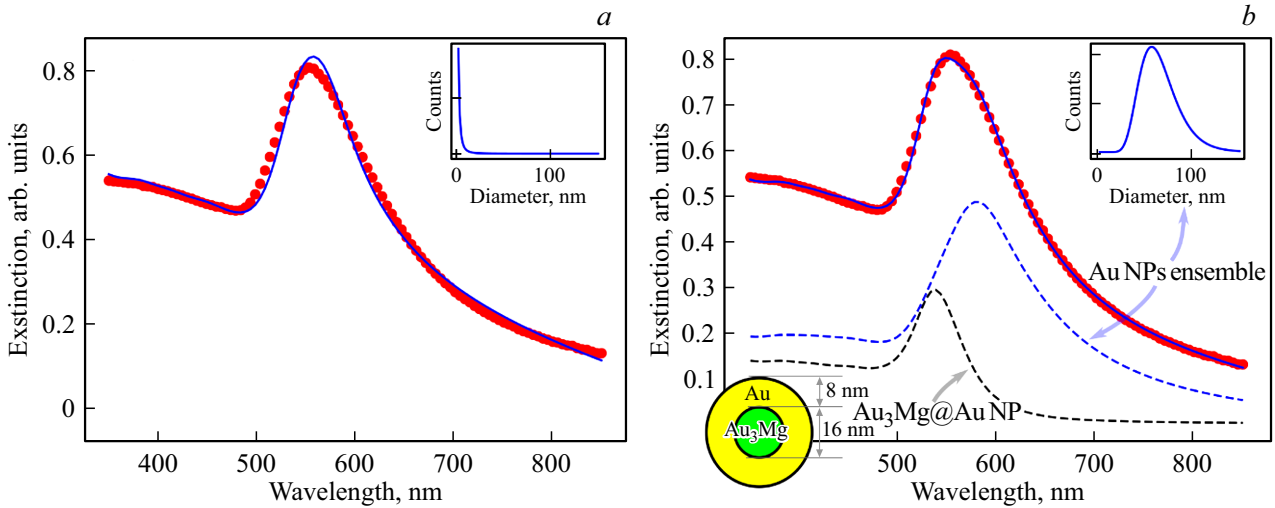


Figure 5. Results of fitting the experimental extinction spectrum of the AuMg/glass sample (red dots) with models of nanoparticles of various compositions and sizes: (a) monometallic gold nanoparticles with their diameters distributed as shown in the inset; (b) gold nanoparticles combined with nanoparticles having an $Au_3Mg@Au$ structure (Au_3Mg core and Au shell) with their diameters distributed as shown in the inset.

size distribution of gold nanoparticles (see the inset in Fig. 5, a), which failed to provide even a remotely faithful reproduction of experimental data. The comparison of extinction spectra in Fig. 5 suggests that model contributions of pure gold nanoparticles and their ensembles in glass are not sufficient to characterize the experimental spectrum.

In order to obtain a better fit to the experimental extinction spectrum of the examined AuMg/glass nanocomposite, contributions of monodisperse nanoparticles, such as magnesium particles and AuMg particles with an alloy or core-shell structure, were added to the dominant contribution of an ensemble of gold nanoparticles. The weight fraction and characteristics of monodisperse nanoparticles (their size

and the core size for composite particles) were varied together with the parameters of the ensemble of gold nanoparticles. The best fit (see Fig. 5, *b*) was obtained when the contribution of the ensemble of gold nanoparticles was summed with the contribution of particles with a core@shell structure (a gold shell and an Au₃Mg alloy core). The fitting procedure yielded a realistic size distribution of „background“ gold nanoparticles with a mean diameter of ~ 60 nm and provided an estimate of the size of composite nanoparticles: 8 and 16 nm for the core and shell diameters, respectively.

4. Conclusion

The following facts were established by applying density functional theory with a Hubbard correction (DFT+U) to gold, magnesium, a series of alloys of these materials, and AuMg nanoparticles.

The use of Hubbard parameter $U = 2.5$ eV for gold atoms within the LDA+U approach allows one to characterize the extinction spectra of gold nanoparticles. The wavelength and the intensity of localized plasmon resonance may then be determined with an error of ~ 10 nm and ~ 18%, respectively.

The calculated formation energies indicate that the AuMg alloy with a CsCl structure has an energetic advantage over other alloys. The extinction spectra of nanoparticles of Au_{*x*}Mg_{1-*x*} alloys at gold concentrations $x < 50\%$ are close to the spectra of pure magnesium nanoparticles.

The Au₃Mg alloy with a *Cmcm* structure holds the most promise for production of broadband light absorbers.

Calculated refraction indices were used to determine the structural features of a material synthesized in the process of laser melting of a film that contained gold and magnesium and was positioned on glass. The best fit to the experimental extinction spectrum revealed that both an ensemble of gold nanoparticles and composite nanoparticles with an Au₃Mg alloy core and a gold shell were present in this composite material.

Acknowledgments

The authors wish to thank Dr. Jürgen Ihlemann (Institute for Nanophotonics Göttingen, Germany) for sample preparation and recording of spectra.

Funding

This study was supported by grant No. 22-12-00106 from the Russian Science Foundation, <https://rscf.ru/project/22-12-00106/>.

Conflict of interest

The authors declare that they have no conflict of interest.

References

- [1] V. Amendola, R. Pilot, M. Frascioni, O.M. Maragó, M.A. Iatí. *J. Phys. Cond. Matt.*, **29**, 203002 (2017). DOI: 10.1088/1361-648X/aa60f3
- [2] E.S. Babich, E.S. Gangrskaiia, I.V. Reduto, J. Béal, A.V. Redkov, T. Maurer, A.A. Lipovskii. *Curr. Appl. Phys.*, **19**, 1088–1095 (2019). DOI: 10.1016/j.cap.2019.07.003
- [3] L. Tong, T. Zhua, Z. Liu. *Chem. Soc. Rev.*, **40**, 1296–1304 (2011). DOI: 10.1039/c001054p
- [4] J.U. Kim, S. Lee, S.J. Kang, T. Kim. *Nanoscale*, **10**, 21555–21574 (2018). DOI: 10.1039/C8NR06024J
- [5] J.R. Mejía-Salazar, O.N. Oliveira. *Chem. Rev.*, **118**,
- [6] G. Baffou, R. Quidant. *Chem. Soc. Rev.*, **43**, 3898 (2014). DOI: 10.1039/c3cs60364d
- [7] M.I. Stockman, K. Kneipp, S.I. Bozhevolnyi, S. Saha, A. Dutta, J. Ndukaife, N. Kinsey, H. Reddy, U. Guler, V.M. Shalaev, A. Boltasseva, B. Gholipour, H.N.S. Krishnamoorthy, K.F. MacDonald, C. Soci, N.I. Zheludev, V. Savinov, R. Singh, P. Groß, C. Lienau, M. Vadai, M.L. Solomon, D.R. Barton, M. Lawrence, J.A. Dionne, S.V. Boriskina, R. Esteban, J. Aizpurua, X. Zhang, S. Yang, D. Wang, W. Wang, T.W. Odom, N. Accanto, P.M. de Roque, I.M. Hancu, L. Piatkowski, N.F. van Hulst, M.F. Kling. *J. Opt.*, **20**, 043001 (2018). DOI: 10.1088/2040-8986/aaa114
- [8] E.S. Sazali, M.R. Sahar, S.K. Ghoshal, R. Arifin, M.S. Rohani, A. Awang. *J. Alloys Compd.*, **607**, 85–90 (2014). DOI: 10.1016/j.jallcom.2014.03.175
- [9] M.A. Garcia. *J. Phys. D.*, **44**, 283001 (2011). DOI: 10.1088/0022-3727/44/28/283001
- [10] O.A. Yeshchenko, I.M. Dmitruk, A.A. Alexeenko, M.Y. Losytskyy, A.V. Kotko, A.O. Pinchuk. *Phys. Rev. B*, **79**, 235438 (2009). DOI: 10.1103/PhysRevB.79.235438
- [11] G.H. Chan, J. Zhao, E.M. Hicks, G.C. Schatz, R.P. Van Duyne. *Nano Lett.*, **7**, 1947–1952 (2007). DOI: 10.1021/nl070648a
- [12] Y. Gutiérrez, D. Ortiz, J.M. Sanz, J.M. Saiz, F. Gonzalez, H.O. Everitt, F. Moreno. *Opt. Express*, **24**, 20621 (2016). DOI: 10.1364/OE.24.020621
- [13] Y. Gutiérrez, M. Losurdo, P. García-Fernández, M. Sainz de la Maza, F. González, A.S. Brown, H.O. Everitt, J. Junquera, F. Moreno. *Opt. Mater. Express*, **9**, 4050 (2019). DOI: 10.1364/OME.9.004050
- [14] J.S. Biggins, S. Yazdi, E. Ringe. *Nano Lett.*, **18**, 3752–3758 (2018). DOI: 10.1021/acs.nanolett.8b00955
- [15] M.Y. Gutkin, A.L. Kolesnikova, S.A. Krasnitsky, A.E. Romanov. *Phys. Solid State*, **56**, 723–730 (2014). DOI: 10.1134/S1063783414040106
- [16] A.A. Antipov, S.M. Arakelian, S.V. Kutrovskaya, A.O. Kucherik, T.A. Vartanian. *Opt. Spectrosc.*, **116**, 324–327 (2014). DOI: 10.1134/S0030400X14020039
- [17] C. Gong, M.S. Leite. *ACS Photonics*, **3**, 507?513 (2016). DOI: 10.1021/acsphotonics.5b00586
- [18] M.-H. Chiu, J.-H. Li, T. Nagao. *Micromachines*, **10**, 73 (2019). DOI: 10.3390/mi10010073
- [19] M. Heinz, V. V. Srabionyan, L.A. Avakyan, A.L. Bugaev, A.V. Skidanenko, S.Y. Kapteelinin, J. Ihlemann, J. Meinertz, C. Patzig, M. Dubiel, L.A. Bugaev. *J. Alloys Compd.*, **767**, 1253–1263 (2018). DOI: 10.1016/j.jallcom.2018.07.183
- [20] Z. Nemati, J. Alonso, H. Khurshid, M.H. Phan, H. Srikanth. *RSC Adv.*, **6**, 38697–38702 (2016). DOI: 10.1039/C6RA05064F

- [21] A.V. Skidanenko, L.A. Avakyan, E.A. Kozinkina, L.A. Bugaev. *Phys. Solid State*, **60**, 2571–2578 (2018). DOI: 10.1134/S1063783419010256.
- [22] L. Avakyan, V. Durimanov, D. Nemesh, V. Srabionyan, J. Ihlemann, L. Bugaev. *Opt. Mater. (Amst.)*, **109**, 110264 (2020). DOI: 10.1016/j.optmat.2020.110264
- [23] P. Giannozzi, S. Baroni, N. Bonini, M. Calandra, R. Car, C. Cavazzoni, D. Ceresoli, G.L. Chiarotti, M. Cococcioni, I. Dabo, A. Dal Corso, S. de Gironcoli, S. Fabris, G. Fratesi, R. Gebauer, U. Gerstmann, C. Gougoussis, A. Kokalj, M. Lazzeri, L. Martin-Samos, N. Marzari, F. Mauri, R. Mazzarello, S. Paolini, A. Pasquarello, L. Paulatto, C. Sbraccia, S. Scandolo, G. Sclauzero, A.P. Seitsonen, A. Smogunov, P. Umari, R.M. Wentzcovitch. *J. Phys. Cond. Matt.*, **21**, 395502 (2009). DOI: 10.1088/0953-8984/21/39/395502
- [24] I. Timrov, N. Marzari, M. Cococcioni. *Phys. Rev. B*, **98**, 085127 (2018). DOI: 10.1103/PhysRevB.98.085127
- [25] J. Enkovaara, C. Rostgaard, J.J. Mortensen, J. Chen, M. Dułak, L. Ferrighi, J. Gavnholt, C. Glinsvad, V. Haikola, H.A. Hansen, H.H. Kristoffersen, M. Kuisma, A.H. Larsen, L. Lehtovaara, M. Ljungberg, O. Lopez-Acevedo, P.G. Moses, J. Ojanen, T. Olsen, V. Petzold, N.A. Romero, J. Stausholm-Møller, M. Strange, G.A. Tritsarlis, M. Vanin, M. Walter, B. Hammer, H. Häkkinen, G.K.H. Madsen, R.M. Nieminen, J.K. Nørskov, M. Puska, T.T. Rantala, J. Schiøtz, K.S. Thygesen, K.W. Jacobsen. *J. Phys. Cond. Matt.*, **22**, 253202 (2010). DOI: 10.1088/0953-8984/22/25/253202
- [26] S. Gražulis, A. Daškevič, A. Merkys, D. Chateigner, L. Lutterotti, M. Quirós, N.R. Serebryanaya, P. Moeck, R.T. Downs, A. Le Bail. *Nucleic Acids Res.*, **40**, D420–D427 (2012). DOI: 10.1093/nar/gkr900
- [27] D.R. Hamann. *Phys. Rev. B*, **88**, 085117 (2013). DOI: 10.1103/PhysRevB.88.085117
- [28] D.W. Mackowski, M.I. Mishchenko. *J. Quant. Spectrosc. Radiat. Transf.*, **112**, 2182–2192 (2011). DOI: 10.1016/j.jqsrt.2011.02.019
- [29] L.A. Avakyan, M. Heinz, A. V. Skidanenko, K.A. Yablunovskii, J. Ihlemann, J. Meinertz, C. Patzig, M. Dubiel, L.A. Bugaev. *J. Phys. Cond. Matt.*, **30**, 045901 (2018). DOI: 10.1088/1361-648X/aa9fcc
- [30] S.A. Tolba, K.M. Gameel, B.A. Ali, H.A. Almossalami, N.K. Allam. *The DFT+U: Approaches, Accuracy, and Applications*, in: *Density Funct. Calc. — Recent Progresses Theory Appl.*, InTech, 2018. DOI: 10.5772/intechopen.72020
- [31] D. Rioux, S. Vallières, S. Besner, P. Muñoz, E. Mazur, M. Meunier. *Adv. Opt. Mater.*, **2**, 176–182 (2014). DOI: 10.1002/adom.201300457
- [32] H.-J. Hagemann, W. Gudat, C. Kunz. *JOSA*, **65**, 742 (1975). DOI: 10.1364/JOSA.65.000742
- [33] L. Gamez-Mendoza, M.W. Terban, S.J.L. Billinge, M. Martinez-Inesta. *J. Appl. Crystallogr.*, **50**, 741–748 (2017). DOI: 10.1107/S1600576717003715

Translated by D.Safin